Eur. Phys. J. Spec. Top.
https://doi.org/10.1140/epjs/s11734-023-00949-8

THE EUROPEAN PHYSICAL JOURNAL SPECIAL TOPICS

Regular Article

Efficiency and thermodynamic uncertainty relations of a dynamical quantum heat engine

Luca Razzoli[1,2,a], Fabio Cavaliere[3,4,b], Matteo Carrega[4,c], Maura Sassetti[3,4,d], and Giuliano Benenti[1,2,5,e]

[1] Center for Nonlinear and Complex Systems, Dipartimento di Scienza e Alta Tecnologia, Università degli Studi dell'Insubria, Via Valleggio 11, 22100 Como, Italy
[2] Istituto Nazionale di Fisica Nucleare, Sezione di Milano, Via Celoria 16, 20133 Milan, Italy
[3] Dipartimento di Fisica, Università di Genova, Via Dodecaneso 33, 16146 Genoa, Italy
[4] CNR-SPIN, Via Dodecaneso 33, 16146 Genoa, Italy
[5] NEST, Istituto Nanoscienze-CNR, Piazza S. Silvestro 12, 56127 Pisa, Italy

Received 28 March 2023 / Accepted 19 July 2023

Abstract In the quest for high-performance quantum thermal machines, looking for an optimal thermodynamic efficiency is only part of the issue. Indeed, at the level of quantum devices, fluctuations become extremely relevant and need to be taken into account. In this paper we study the thermodynamic uncertainty relations for a quantum thermal machine with a quantum harmonic oscillator as a working medium, connected to two thermal baths, one of which is dynamically coupled. We show that parameters can be found such that the machine operates both as a quantum engine or refrigerator, with both sizeable efficiency and small fluctuations.

1 Introduction

The rapid development of quantum technologies calls for a deeper understanding of thermodynamics and energetics at a microscopic level, where unavoidable quantum effects have to be taken into account. The extension of classical concepts of thermodynamics to the quantum realm is not only at the forefront of fundamental theoretical research [1–6], but also relevant for new nanodevice applications [7–12]. Mastering the thermodynamics of quantum systems far from equilibrium, from energy storage to energy transfer and transduction and heat–to–work conversion, is of great importance for emerging technologies with applications in quantum computing [12–14], quantum communication [15, 16], and quantum sensing [17].

Spurred by the rapid emergence of new quantum technology platforms, in the last few years the first prototype realizations of quantum thermal machines [11, 18–21] and quantum batteries [22, 23] have been reported, calling for new theoretical and experimental investigations, even including extensions to non-Hermitian quantum thermodynamics [24, 25]. For instance, a great interest revolves around heat nanoengines and refrigerators where the working medium (WM) is a quantum system coupled to several thermal reservoirs. Indeed, it has been shown that a multiterminal configuration can improve both the output power and the efficiency at maximum power [26–35]. Also, the impact of quantum coherence on the performance of thermal machines has been inspected [36–45], as well as the role of the uncertainty principle [46].

Quantum devices are highly sensitive to fluctuations that may limit device performances [4, 19, 47–49], in contrast to macroscopic devices, where usually fluctuations can be safely neglected. To assess fluctuations, the thermodynamic uncertainty relations (TURs) have been recently introduced [50–60] and a unified toolbox for describing current fluctuations in the context of open quantum systems has been proposed [61]. These TURs combine steady-state currents J, their fluctuations D_J and dissipation (measured by the entropy production rate $\dot{S}$), giving limits on the precision of currents for a given dissipation. Indeed, in Ref. [50] it was reported that for certain classical Markovian systems, the signal-to-noise ratio satisfies a TUR bound, showing that relative current fluctuations are lower bounded in

Fabio Cavaliere, Matteo Carrega, Maura Sassetti and Giuliano Benenti have contributed equally to this work.

[a] e-mail: luca.razzoli@uninsubria.it (corresponding author)
[b] e-mail: fabio.cavaliere@unige.it
[c] e-mail: matteo.carrega@spin.cnr.it
[d] e-mail: maura.sassetti@unige.it
[e] e-mail: giuliano.benenti@uninsubria.it

Published online: 07 August 2023

terms of the inverse entropy production rate. By introducing a dimensionless trade-off parameter Q_J, TURs can be expressed as

$$Q_J \equiv \dot{S}\frac{D_J}{J^2} \geq 2k_B, \tag{1}$$

where k_B is the Boltzmann constant (from now on we will set $k_B = 1$). After that, several bounds for TURs [62–70], and their possible violations, have been put forward under different assumptions, starting from classical Markovian dynamics to quantum systems, including time-dependent forces and the role of time-reversal symmetry. For instance, when the model preserves time–reversal–symmetry it has been shown that, at least in the linear regime [57, 65], the trade-off parameter Q never achieves values lower than 2. Recently, experimental results on TURs have appeared [55]. They thus represent new tools to inspect the performances of so-far unexplored resources based on non-thermal states, correlations and quantum coherences in non-equilibrium quantum systems [47].

In this work, we propose a physically implementable quantum thermal machine and investigate its operation. We consider a single quantum harmonic oscillator, a paradigmatic model and a building block of many quantum technologies [12, 13, 71–77], as the WM coupled to two thermal reservoirs. One of them is statically linked, while the other one is modulated at a frequency Ω (monochromatic driving). Driven system-bath couplings offer enhanced design flexibility, such as the possibility to switch between regimes of quantum heat engine or refrigerator [33, 78]. Here we are interested in assessing the precision of the currents in such regimes, by studying the TURs related to the heat current and the work current (i.e., the total exchanged power). Via a systematic perturbative approach, we obtain expressions for the thermodynamic quantities and the TURs, that can be numerically integrated with standard techniques. Even though we report no violation of TURs, i.e., we do not observe values of $Q < 2$, we show that Q can attain minimal values (close to 2) both in the engine and refrigerator regimes, accompanied by sizeable efficiency. Values $Q \approx 2$ are related to a nearly optimal trade-off of the three desiderata we commonly want for a heat engine (refrigerator)—finite output power (cooling power), efficiency (coefficient of performance) close to the Carnot value, and small fluctuations—as Q can be explicitly written in terms of them [63]. In the limit of very small damping, simple analytical expressions for the TURs are obtained, which support our findings.

In Sect. 2 the model is illustrated, along with the definition of all thermodynamic quantities and corresponding correlators describing their fluctuations. We then evaluate their quantum and time averaged values in the dynamical steady state, to lowest order in the strength of the dynamical coupling. Results are reported and discussed in Sect. 3, and conclusions are drawn in Sect. 4. Appendix A provides details on the adopted perturbative approach, while Appendix B illustrates all the possible operating modes of the proposed quantum thermal machine.

2 Model and general setting

2.1 Model

We consider a minimal model for an operating heat engine in the quantum regime. A single quantum harmonic oscillator acts as the WM and is coupled to two thermal reservoirs, respectively kept at temperatures T_1 and T_2 –see Fig. 1. The total Hamiltonian is ($\hbar = k_B = 1$)

$$H^{(t)} = H_{\rm WM} + \sum_{\nu=1}^{2}\Big[H_\nu + H^{(t)}_{{\rm int},\nu}\Big], \tag{2}$$

where the Hamiltonian of the WM is

$$H_{\rm WM} = \frac{p^2}{2m} + \frac{1}{2}m\omega_0^2 x^2, \tag{3}$$

with m and ω_0 the mass and the characteristic frequency. The Hamiltonian of the $\nu = 1, 2$ reservoir is described in the usual Caldeira-Legget framework [79, 80] in terms of an infinite set of independent harmonic oscillators as

$$H_\nu = \sum_{k=1}^{+\infty}\left[\frac{P^2_{k,\nu}}{2m_{k,\nu}} + \frac{1}{2}m_{k,\nu}\omega^2_{k,\nu}X^2_{k,\nu}\right], \tag{4}$$

and the interaction between the WM and the ν–th reservoir is

$$H^{(t)}_{{\rm int},\nu} = \sum_{k=1}^{+\infty}\left[-g_\nu(t)c_{k,\nu}xX_{k,\nu} + \frac{g^2_\nu(t)c^2_{k,\nu}}{2m_{k,\nu}\omega^2_{k,\nu}}x^2\right], \tag{5}$$

where $c_{k,\nu}$ describes the interaction strength and the counter–term $\propto x^2$ prevents the renormalization of the WM potential. Following Refs. [33, 78, 81], we focus on a dynamical coupling situation to establish a working

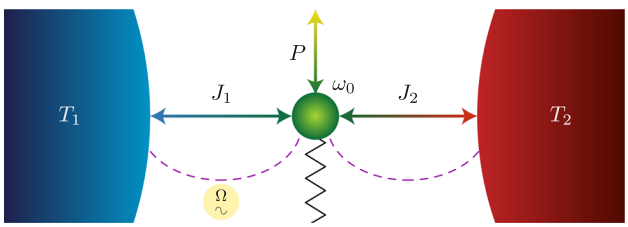

Fig. 1 Setup. Schematic depiction of the setup under investigation. The WM – a quantum harmonic oscillator with characteristic frequency ω_0 – is in contact with two thermal reservoirs at temperatures T_ν, with $\nu = 1, 2$. The WM can exchange heat currents J_ν with the reservoirs and total power P with an external source. The purple dashed lines represent the coupling between the WM and the thermal reservoirs. The coupling to the $\nu = 1$ reservoir is modulated in time with frequency Ω, while that to the $\nu = 2$ reservoir is static

thermal machine in a periodic steady state regime. In particular, we assume here that the dimensionless coupling to the $\nu = 1$ reservoir is modulated in time as $g_1(t) = \cos(\Omega t)$, with Ω the driving frequency, while the $\nu = 2$ coupling is kept constant $g_2(t) = 1$ – see the sketch in Fig. 1. At the initial time $t_0 \to -\infty$, the reservoirs are assumed in their thermal equilibrium at temperatures T_ν, with the total density matrix written in a factorized form as

$$\rho(t_0) = \rho_{\rm WM}(t_0) \otimes \rho_1(t_0) \otimes \rho_2(t_0), \tag{6}$$

with

$$\rho_\nu(t_0) = \frac{e^{-H_\nu/T_\nu}}{{\rm Tr}\{e^{-H_\nu/T_\nu}\}} \tag{7}$$

and with $\rho_{\rm WM}(t_0)$ the initial density matrix of the WM.

In the Heisenberg picture the equations of motion for the WM and reservoir degrees of freedom [81] are, respectively,

$$\begin{aligned}
\dot{x}(t) &= \frac{p(t)}{m}, \\
\dot{p}(t) &= -m\omega_0^2 x(t) + \sum_{\nu=1}^{2}\sum_{k=1}^{+\infty}\Big[g_\nu(t)c_{k,\nu}X_{k,\nu}(t) \\
&\quad - \frac{g_\nu^2(t)c_{k,\nu}^2}{m_{k,\nu}\omega_{k,\nu}^2}x(t)\Big],
\end{aligned} \tag{8}$$

and

$$\begin{aligned}
\dot{X}_{k,\nu}(t) &= \frac{P_{k,\nu}(t)}{m_{k,\nu}}, \\
\dot{P}_{k,\nu}(t) &= -m_{k,\nu}\omega_{k,\nu}^2 X_{k,\nu}(t) + g_\nu(t)c_{k,\nu}x(t),
\end{aligned} \tag{9}$$

where overdots denote time derivatives.

The solution for the position operator of the k–th oscillator of the ν–th reservoir is

$$\begin{aligned}
X_{k,\nu}(t) &= \xi_{k,\nu}(t) + \frac{c_{k,\nu}}{m_{k,\nu}\omega_{k,\nu}}\cdot \\
&\quad \cdot \int_{t_0}^{t} {\rm d}s\; g_\nu(s)x(s)\sin[\omega_{k,\nu}(t-s)]\,,
\end{aligned} \tag{10}$$

$$\begin{aligned}
\xi_{k,\nu}(t) &= X_{k,\nu}(t_0)\cos[\omega_{k,\nu}(t-t_0)] \\
&\quad + \frac{P_{k,\nu}(t_0)}{m_{k,\nu}\omega_{k,\nu}}\sin[\omega_{k,\nu}(t-t_0)].
\end{aligned} \tag{11}$$

The usual fluctuating force operator, a stochastic force which the reservoir exerts on the WM and that obeys stationary Gaussian statistics, is defined as [79]

$$\xi_\nu(t) \equiv \sum_{k=1}^{+\infty} c_{k,\nu}\xi_{k,\nu}(t), \tag{12}$$

with zero quantum average $\langle\xi_\nu(t)\rangle = {\rm Tr}\{\xi_\nu(t)\rho(t_0)\} = 0$ and correlation function $\langle\xi_\nu(t)\xi_{\nu'}(t')\rangle \equiv \mathcal{L}_\nu(t-t')\delta_{\nu,\nu'}$, with

$$\mathcal{L}_\nu(t-t') = \mathcal{L}_{\nu,\rm s}(t-t') + \mathcal{L}_{\nu,\rm a}(t-t'). \tag{13}$$

Here, the symmetric (s) and anti-symmetric (a) contributions with respect to the time argument are

$$\mathcal{L}_{\nu,\rm s}(t) = \int_0^{+\infty}\frac{{\rm d}\omega}{\pi}\mathcal{J}_\nu(\omega)\coth\left(\frac{\omega}{2T_\nu}\right)\cos(\omega t), \tag{14}$$

$$\mathcal{L}_{\nu,\rm a}(t) = -i\int_0^{+\infty}\frac{{\rm d}\omega}{\pi}\mathcal{J}_\nu(\omega)\sin(\omega t). \tag{15}$$

In the above expressions, the so-called spectral density [79]

$$\mathcal{J}_\nu(\omega) = \frac{\pi}{2}\sum_{k=1}^{+\infty}\frac{c_{k,\nu}^2}{m_{k,\nu}\omega_{k,\nu}}\delta(\omega-\omega_{k,\nu}) \tag{16}$$

has been introduced. It governs the properties of the ν–th reservoir, e.g. its possible non–Markovian behaviour [82–86]. The precise shape of $\mathcal{J}_\nu(\omega)$ will be specified later.

2.2 Thermodynamic quantities

In this work we focus on thermodynamic quantities in the long time limit, when a periodic steady state has been reached. Therefore, all quantities of interest can be averaged over one period of the drive $\mathcal{T} = 2\pi/\Omega$, and are therefore well-defined both for weak and strong coupling [87–90]. The average heat current J_ν of the ν–th reservoir and the total power P can be written as [78]

$$P = \frac{1}{\mathcal{T}}\int_{\bar{t}}^{\bar{t}+\mathcal{T}}{\rm d}t'\sum_{\nu=1}^{2}{\rm Tr}\left[\frac{\partial H_{{\rm int},\nu}^{(t')}}{\partial t'}\rho(t')\right], \tag{17}$$

$$J_\nu = -\frac{1}{\mathcal{T}}\int_{\bar{t}}^{\bar{t}+\mathcal{T}}{\rm d}t'{\rm Tr}\left[H_\nu\frac{\rm d}{{\rm d}t'}\rho(t')\right], \tag{18}$$

where $\rho(t)$ is the total density matrix, describing the WM plus reservoirs at time t, and, here and in the following, $\bar{t}$ denotes a large positive time. It is worth noting that a positive sign in the above quantities indicates an energy flow towards the WM. Since the power contribution is associated to the temporal variation of the interaction term, it is only due to the dynamical coupling of the WM to the $\nu = 1$ bath. An energy balance relation holds true,

$$P + J_1 + J_2 = 0, \tag{19}$$

reflecting the first law of thermodynamics [6, 47, 78]. An important quantity to assess the thermodynamic

performances is the time–averaged entropy production rate, related to the heat currents by [6, 47, 88]

$$\dot{S} = -\sum_{\nu=1}^{2} \frac{J_\nu}{T_\nu}, \tag{20}$$

with $\dot{S} \geq 0$ in accordance to the second law of thermodynamics [47].

Due to dissipation, all quantities undergo fluctuations that affect the device performances. During the whole time interval $t-t_0$, fluctuations can be characterized by auto–correlation functions [57, 79]: Given an observable $O(t)$ we define

$$D_O(t) = \frac{1}{t-t_0}\int_{t_0}^{t} \mathrm{d}s \int_{t_0}^{t} \mathrm{d}s' \langle O(s)O(s')\rangle, \tag{21}$$

where $t - t_0$ is a large time interval, $t - t_0 \to +\infty$, and where $\langle A(t)\rangle \equiv \mathrm{Tr}\{A(t)\rho(t_0)\}$ denotes the quantum average. In this limit, the above auto–correlation function reduces to a single integral, that can be written as [57]

$$D_O(t) = \int_0^{+\infty} \mathrm{d}\tau \langle \{O(t), O(t-\tau)\}\rangle, \tag{22}$$

with $\{A, B\} = AB + BA$ the anti–commutator, leading to the period–averaged fluctuations

$$D_O = \frac{1}{\mathcal{T}}\int_{\bar{t}}^{\bar{t}+\mathcal{T}} \mathrm{d}s\ D_O(s). \tag{23}$$

3 Results

The dynamics of the driven dissipative quantum system can be solved by resorting to non-equilibrium Green function formalism [91–93], as described in Ref. [81]. In this work, however, we will only focus on the case in which the modulated coupling ($\nu = 1$) is much weaker than the static one ($\nu = 2$). Under these circumstances, a perturbative expansion can be used to evaluate all the quantities introduced above. To do so, it is convenient to rewrite the total Hamiltonian in Eq. (2) as

$$H^{(t)} = H^{(0)} + \Delta H^{(t)}, \tag{24}$$

as the sum of an unperturbed Hamiltonian, $H^{(0)}$, and $\Delta H^{(t)}$, the time–dependent interaction with the reservoir $\nu = 1$:

$$H^{(0)} = H_{\mathrm{WM}} + \sum_{\nu=1}^{2} H_\nu + H_{\mathrm{int},2};\ \Delta H^{(t)} = H^{(t)}_{\mathrm{int},1}.$$

Deferring all details to Appendix A, here we quote the final results for the quantities of interest defined in Sect. 2.2 and obtained at the lowest-order perturbative correction. The total power P and the heat current J_1 are

$$P = -\Omega \int_{-\infty}^{+\infty} \frac{\mathrm{d}\omega}{4\pi m} \mathcal{J}_1(\omega+\Omega) N(\omega) \chi_0''(\omega), \tag{25}$$

$$J_1 = \int_{-\infty}^{+\infty} \frac{\mathrm{d}\omega}{4\pi m} (\omega+\Omega) \mathcal{J}_1(\omega+\Omega) N(\omega) \chi_0''(\omega), \tag{26}$$

where we have introduced

$$N(\omega) = \coth\left(\frac{\omega+\Omega}{2T_1}\right) - \coth\left(\frac{\omega}{2T_2}\right) \tag{27}$$

and the response function $\chi_0(t)$ (see Appendix A) whose Fourier transform is

$$\chi_0(\omega) = -\frac{1}{\omega^2 - \omega_0^2 + i\omega\gamma_2(\omega)}, \tag{28}$$

where $\gamma_2(\omega) = \int_{-\infty}^{+\infty} \mathrm{d}t e^{i\omega t}\gamma_2(t)$ is the damping kernel of the $\nu = 2$ bath in Fourier space with

$$\gamma_\nu(t) \equiv \sum_{k=1}^{+\infty} \frac{c_{k,\nu}^2}{m_{k,\nu}\omega_{k,\nu}^2} \cos(\omega_{k,\nu} t). \tag{29}$$

Here and in the following the double prime denotes the imaginary part. In the following we will focus only on J_1 and P, but J_2 can be easily obtained from the energy balance expressed by Eq. (19). The auto–correlation functions for the total power, D_P, and for the heat current, D_{J_1}, are

$$D_P = \Omega^2 \int_{-\infty}^{+\infty} \frac{\mathrm{d}\omega}{4\pi m}\ \mathcal{J}_1(\omega+\Omega) R(\omega) \chi_0''(\omega), \tag{30}$$

$$D_{J_1} = \int_{-\infty}^{+\infty} \frac{\mathrm{d}\omega}{4\pi m} (\omega+\Omega)^2 \mathcal{J}_1(\omega+\Omega) R(\omega) \chi_0''(\omega), \tag{31}$$

with

$$R(\omega) = \coth\left(\frac{\omega+\Omega}{2T_1}\right)\coth\left(\frac{\omega}{2T_2}\right) - 1. \tag{32}$$

Hereafter, we focus on the specific case of a system with a structured, Lorentzian spectral density for the dynamically coupled bath

$$\mathcal{J}_1(\omega) = \frac{d_1 m \gamma_1 \omega}{(\omega^2 - \omega_1^2)^2 + \gamma_1^2\omega^2}, \tag{33}$$

peaked at $\omega \approx \omega_1$, with typical broadening γ_1, and coupling strength parameterized by d_1. Such a spectral density offers a great versatility, i.e., exploiting

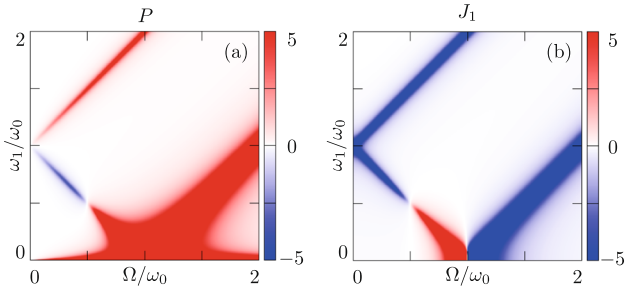

Fig. 2 Energy currents and operating modes. Panels **a** and **b** show, as a density plot, the average power P and heat current J_1 as a function of the driving frequency Ω and the resonance frequency ω_1. Both quantities are here normalized to γ_2^2. The dashed line marks the resonance condition $\omega_1 = \omega_0 - \Omega$. In all panels $T_1 = 0.4\omega_0$, $T_2 = 0.8\omega_0$, $\gamma_1 = 0.05\omega_0$, $\gamma_2 = 0.01\omega_0$, and $d_1 = 10^{-3}\omega_0^4$

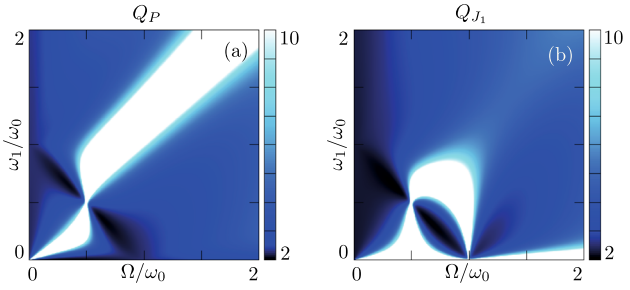

Fig. 3 Quantifying fluctuations via TURs. Density plot of Q_P (**a**) and Q_{J_1} (**b**) as a function of Ω and ω_1. Parameters as in Fig. 2

different resonant conditions between external drive Ω and ω_1, and is known to induce non–Markovian effects [78, 82–86], a necessary condition to have a dynamical heat engine in this setup [78]. In the case of a Ohmic spectral density, instead, the present quantum thermal machine would not operate as heat engine [78]. A Lorentzian spectral density can be either obtained in cavity–optomechanical systems [71, 72] or in circuit-QED setups [73, 94], with the latter representing a particularly convenient solid–state platform which allows to tune dynamical couplings up to a high degree of precision [95]. For the statically coupled contact we choose a Ohmic spectral density $\mathcal{J}_2(\omega) = m\gamma_2\omega$, which implies $\gamma_2(\omega) \equiv \gamma_2$ in Eq. (28).

3.1 Average thermodynamic quantities

The quantum-thermodynamical properties of this setup have been investigated recently [78]. It has been shown that it can either operate as a quantum engine or a quantum refrigerator depending on the parameters. Here we focus on the case $\gamma_{1,2} \ll \omega_0$, favourable to obtain better performances and smaller fluctuations, and on temperatures in the quantum regime $T_\nu < \omega_0$. In particular, we show here the case $T_2 = 2T_1$, with $T_1 = 0.4\omega_0$.[1]

Results for the total power P and for the heat current J_1, obtained by numerically integrating Eqs. (25),(26) are shown as density plots in Fig. 2a, b as a function of the driving frequency Ω and ω_1. Depending on the sign of J_ν and P different operating modes are identified (see Appendix B) [33]. Here we focus on the most relevant ones: Heat engine with $P < 0$ and $J_1 < 0$ and refrigerator with $P > 0$ and $J_1 > 0$. The best performance for these operating modes occurs, for $T_1 < T_2$, when $\omega_1 = \omega_0 - \Omega$ is satisfied [78], see the dashed line.[2]

We mention that the performance of proposed dynamical quantum heat engine has been investigated beyond the weak-coupling regime in Sect. IV.C of Ref. [78]. In that regime, we observe a broadening of the power resonance line, which appears to be detuned with respect to $\omega_1 = \omega_0 - \Omega$, and it is possible to achieve sensibly larger power outputs. However, higher efficiency is observed in the weak-coupling regime. The heat engine is lost in the limit of very strong coupling.

3.2 Thermodynamic uncertainty relations

It is now interesting to assess the impact of fluctuations on the performance of this setup. To this end, we use TURs [50, 57, 62, 65, 96]. We are particularly interested in the engine and refrigerator regimes and thus in the TURs for P and J_1, expressed in terms of the trade-off parameter Q_P and Q_{J_1} as [57, 65, 96]

$$Q_P = \dot{S}\frac{D_P}{P^2} \geq 2 \quad Q_{J_1} = \dot{S}\frac{D_{J_1}}{J_1^2} \geq 2. \tag{34}$$

These TURs combine energy flows, their fluctuations, and the entropy production rate in a dimensionless quantity expressing the trade-off between how the system fluctuates with respect to the quality (in terms of magnitude and degree of dissipation) of the energy flow. The lower Q_μ (with $\mu \in \{P, J_1\}$), the better the operation of the thermal machine [63].Figure 3 shows density plots of the numerically evaluated Q_P (a) and Q_{J_1} (b) as a function of Ω and ω_1 and it is clear that $Q_\mu > 2$ everywhere. Via extensive numerical investigations we can report that regardless of all parameter configurations, $Q_\mu < 2$ is never found in this model, and thus no violation of TUR bounds [50, 57, 65] occurs. The trade-off parameters can attain very large values, see the white regions in the plots, and even diverge – e.g.

[1] To be consistent with the perturbative approach, d_1 in Eq. (33) has been chosen small enough so that the peak value of $\mathcal{J}_1(\omega)$ satisfies $\mathcal{J}_1(\omega_1) \ll m\omega_0^2$.

[2] The situation for $T_1 > T_2$ is essentially mirrored along the axis $\omega_1 = \omega_0$. In this case the best engine and refrigerator operating regimes occur along the resonance condition $\omega_1 = \omega_0 + \Omega$ [78].

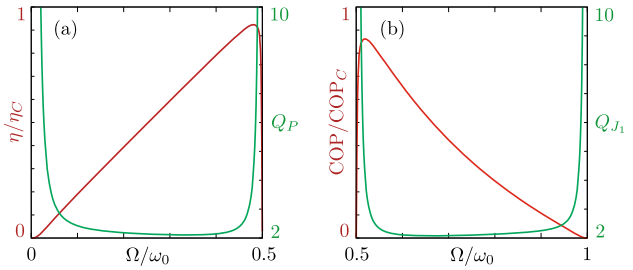

Fig. 4 Efficiency vs. fluctuations. Panel **a** shows as a red curve the efficiency, normalized to the Carnot limit, of the thermal machine operating as an engine, and Q_P as a green line, as a function of Ω along the resonance line $\omega_1 = \omega_0 - \Omega$ – see Fig. 2. Panel **b** shows the same quantities along the same resonance, but in the regime where the machine operates as a refrigerator. Parameters as in Fig. 2

at the crossover between the engine and the refrigerator regimes along $\omega_1 = \omega_0 - \Omega$ (due to J_1, P crossing zero). Interestingly, however, they are instead particularly low (even approaching $Q_\mu \approx 2$) around the latter resonance line, where the best performances occur. Let us then relate Q_μ to the efficiency $\eta = -P/J_2$ (engine mode) or to the coefficient of performance $\mathrm{COP} = J_1/P$ (refrigerator mode), normalized to the respective Carnot limits $\eta_C = 1 - \frac{T_1}{T_2}$ and $\mathrm{COP}_C = \frac{T_1}{T_2 - T_1}$.[3] Figure 4a shows η/η_C (red line) and Q_P (green line) as a function of Ω within the engine region along the dashed line of Fig. 2. As is clear, there is a large range of driving frequencies where Q_P is very close to 2. Furthermore, when it attains its minimum value, for $\Omega \approx 0.35\omega_0$, the efficiency of the engine is $\approx 0.7\eta_C$. On the other hand, when the engine operates at its maximum efficiency of $\eta \approx 0.95\eta_C$, Q_P almost doubles. Notice also that Q_P diverges at the boundaries of the engine regime and that the maximum of η is located in close proximity of one of these edges. The situation in the refrigerator regime is qualitatively similar, and is reported in Fig. 4b. From a different perspective, the trade-off parameter Q_P (Q_{J_1}) in Eq. (34) expresses the performance of the heat engine (refrigerator) as a trade-off between three desiderata [63]: (i) Finite (or even large) average output power $-P > 0$ (cooling power $J_1 > 0$), (ii) an efficiency η (COP) close to the Carnot value η_C (COP_C), and (iii) constancy, i.e., small fluctuations D_P (D_{J_1}). Indeed, we can rewrite Eq. (34) as

$$Q_P = -\frac{1}{T_1}\frac{D_P}{P}\left[\frac{\eta_C}{\eta} - 1\right] \geq 2,$$
$$Q_{J_1} = \frac{1}{T_2}\frac{D_{J_1}}{J_1}\left[\frac{1}{\mathrm{COP}} - \frac{1}{\mathrm{COP}_C}\right] \geq 2, \qquad (35)$$

where, we recall, $T_1 < T_2$. Therefore, attaining values $Q_\mu \approx 2$ means achieving a nearly optimal performance of the machine, intended as a trade-off between the above desiderata.

To gain further insight, we can exploit the fact that in the limit $\gamma_2 \to 0$ one can approximate [78] $\chi_0''(\omega) \approx \frac{\pi}{2\omega_0}\sum_{p=\pm1} p\delta(\omega - p\omega_0)$, with $\delta(\omega)$ the Dirac delta. The integrals in Eqs. (25),(26),(30),(31) are then easily solved, leading to

$$P = -\frac{\Omega}{8m\omega_0}\sum_{p=\pm1} p\mathcal{J}_1(\omega_0 + p\Omega)N_p,$$
$$J_1 = \frac{1}{8m\omega_0}\sum_{p=\pm1} (\omega_0 + p\Omega)\mathcal{J}_1(\omega_0 + p\Omega)N_p,$$
$$D_P = \frac{\Omega^2}{8m\omega_0}\sum_{p=\pm1} \mathcal{J}_1(\omega_0 + p\Omega)R_p,$$
$$D_{J_1} = \frac{1}{8m\omega_0}\sum_{p=\pm1} (\omega_0 + p\Omega)^2\mathcal{J}_1(\omega_0 + p\Omega)R_p,$$

where $N_p = N(p\omega_0)$ and $R_p = R(p\omega_0)$ – see Eqs. (27),(32). In the regime $\gamma_1 \ll \omega_0$ considered in this paper, restricting along the resonance line $\omega_1 = \omega_0 - \Omega$ one can safely drop all terms with $p = +1$ in the above expressions [78]. Then, after simple rearrangements one can see that in this limit $Q_P \equiv Q_{J_1}$, with

$$Q_\mu = 2\left(\frac{\omega_0}{2T_2} - \frac{\omega_0 - \Omega}{2T_1}\right)\coth\left(\frac{\omega_0}{2T_2} - \frac{\omega_0 - \Omega}{2T_1}\right).$$

This proves that, at least in the above limits, the TURs are never violated and $Q_\mu \geq 2$ in agreement with our numerical findings. Indeed, in this limit $Q_\mu = 2$ precisely when $\Omega = \Omega^* = \omega_0\eta_C$, which is the "turning point" between the operation as an engine and that as a refrigerator along the resonance [78]. There, at $\Omega = \Omega^*$, we have $\eta \to \eta_C$ (with $P \to 0$) and $\mathrm{COP} \to \mathrm{COP}_C$ (with $J_1 \to 0$). The net coalescence of engine and refrigerator modes is lifted at finite values of γ_ν, which results in $\eta < \eta_C$ ($\mathrm{COP} < \mathrm{COP}_C$), with the maximum for η (COP) occurring at $\Omega \lesssim \Omega^*$ ($\Omega \gtrsim \Omega^*$). Also, when γ_ν is small but non-zero the trade-off parameters are no longer identical, and develop the divergence near Ω^* seen in Fig. 4.

4 Conclusions

In this paper we have analyzed the fluctuations of the heat current and power exchanged between a quantum thermal machine with a single quantum harmonic oscillator as the WM and two thermal baths at uneven temperature, in the presence of a dynamical coupling between the WM and one of the baths. Such a machine can operate either as a quantum heat engine or as refrigerator depending on the frequency of the drive and the other parameters. To understand the impact of fluctuations on such operating modes we have developed expressions for the fluctuations to leading order in the

[3] For the parameters chosen here, $\eta_C = 0.5$ and $\mathrm{COP}_C = 1$.

amplitude of the dynamical coupling. Such expressions allow us to numerically evaluate the trade-off parameters Q_P and Q_{J_1} associated to total power (in the engine case) or heat current from the cold bath (in the refrigerator case), whose magnitude is associated to the strength and impact of fluctuations. We report no violation of the lower bound proposed for these quantities in the literature. However, we have found that in typical operating regimes the trade-off parameters can reach values very close to the lower bound, implying a nearly optimal trade-off between efficiency (COP), (cooling) power output, and small fluctuations, with an efficiency of about 70% of the Carnot limit in the case of a quantum engine. In the limit of weak damping, appropriate for the regime of parameters considered in this paper, we have also developed an analytical approximation for the trade-off parameters, which supports our findings and shows that TUR bounds cannot be violated in our model, at least for weak damping.

Despite no violation of TURs has been found, showing that the trade-off parameters can attain small values in sensible operating regimes is a first step towards the development of optimal protocols for the operation of quantum thermodynamic machines. Future developments of this work may lead to consider more complex driving protocols for the thermal machine, which could help to even increase the efficiency at the lowest values of the trade-off parameters. Also, it will be interesting to look for more complex quantum thermal machines, either in multi–terminal or multi–WM configurations. Due to their ability to perform multiple thermodynamical tasks at once [33], assessing the impact of fluctuations can be a key issue towards their optimization. As a final outlook, further extensions of the present work may include considering squeezed baths [97–103] to assess if and to which extent performance of the proposed quantum heat machine can be improved by non-thermal baths [104–107].

Acknowledgements L.R. and G.B. acknowledge financial support by the Julian Schwinger Foundation (Grant JSF-21-04-0001) and by INFN through the project 'QUANTUM'. F.C. and M.S. acknowledge support by the "Dipartimento di Eccellenza MIUR 2018-2022."

Funding Open access funding provided by Università degli Studi dell'Insubria within the CRUI-CARE Agreement.

Data availability All data generated during this study have been obtained by numerically implementing the equations presented in the text using standard techniques.

Appendix A: Perturbative approach

In this Appendix we derive the explicit expressions for the average thermodynamic quantities in Eqs. (25), (26), and their auto–correlation functions in Eqs. (30), (31). We start by writing the Hamiltonian as in Eq. (24). In the interaction picture (label I), we freeze out the time evolution generated by $H^{(0)}$, so an observable A is defined as

$$A_{\rm I} = e^{iH^{(0)}(t-t_0)} A_{\rm S} e^{-iH^{(0)}(t-t_0)}, \tag{36}$$

with the label S denoting the Schrödinger picture. Operators in the Heisenberg (label H) and in the interaction picture are related via

$$A_{\rm H}(t) = U_{\rm I}^{\dagger}(t,\, t_0)\, A_{\rm I}(t)\, U_{\rm I}(t,\, t_0), \tag{37}$$

where

$$U_{\rm I}(t,\, t_0) = T \exp\left\{ -i \int_{t_0}^{t} {\rm d}s \Delta H_{\rm I}(s) \right\} \tag{38}$$

is the propagator in the interaction picture, with T the time-ordering symbol. We are interested in the lowest-order perturbative correction with respect to the interaction strength $c_{k,1}$. Recalling that $\Delta H^{(t)} = H^{(t)}_{{\rm int},1}$, given in Eq. (5), according to Eq. (36) we can write

$$\Delta H_{\rm I}(t) \approx -\sum_{k=1}^{+\infty} g_1(t) c_{k,1} x_{\rm I}(t) \xi_{k,1}(t). \tag{39}$$

Indeed, it is possible to show that $X_{k,1;{\rm I}} = \xi_{k,1}(t)$, with $\xi_{k,1}(t)$ defined in Eq. (11). Using Eqs. (12), (37) and considering $U_{\rm I}(t,\, t_0) \approx 1 - i \int_{t_0}^{t} {\rm d}s \Delta H_{\rm I}(s)$, in the Heisenberg picture the position operator of the WM can be written as

$$x(t) = x^{(0)}(t) + \Delta x(t), \tag{40}$$

where $x^{(0)}(t) \equiv x_{\rm I}(t)$ according to Eq. (36) and where the perturbative correction is

$$\Delta x(t) = -i \int_{t_0}^{t} {\rm d}s\, g_1(s) \Big[x^{(0)}(s) \xi_1(s),\, x^{(0)}(t) \Big]. \tag{41}$$

Appendix A.1: Heat current and total power

We start by considering the average heat current J_1. From Eq. (18), as detailed in Ref. [81], we have the general, exact expression

$$J_1 = -\int_{\bar{t}}^{\bar{t}+\mathcal{T}} \frac{\mathrm{d}s}{\mathcal{T}} g_1(s) \Big\langle x(s) \Big[\dot{\xi}_1(s) + \\ + \int_{t_0}^{s} \mathrm{d}s'\, g_1(s') x(s') F_1(s-s') \Big] \Big\rangle, \quad (42)$$

where we have introduced

$$F_1(t) = \sum_{k=1}^{+\infty} \frac{c_{k,1}^2}{m_{k,1}} \cos(\omega_{k,1} t) \quad (43)$$

with Fourier transform $F_1(\omega) = 2\omega \mathcal{J}_1(\omega)$. We obtain the perturbative expansion of Eq. (42),

$$J_1 = -\int_{\bar{t}}^{\bar{t}+\mathcal{T}} \frac{\mathrm{d}s}{\mathcal{T}} g_1(s) \Big\{ \langle x^{(0)}(s) \dot{\xi}_1(s) \rangle + \langle \Delta x(s) \dot{\xi}_1(s) \rangle \\ + \int_{t_0}^{s} \mathrm{d}s'\, g_1(s') \langle x^{(0)}(s) x^{(0)}(s') \rangle F_1(s-s') \Big\}, \quad (44)$$

by expanding $x(t)$ as in Eq. (40) and retaining terms up to $O(c_{k,1}^2)$, as the latter represent the first perturbative correction to J_1. We now perform the quantum average on the initial state of Eq. (6), exploiting the fact that $\langle x^{(0)}(t) \dot{\xi}_1(t) \rangle = 0$ and that

$$\langle \Delta x(t) \dot{\xi}_1(t) \rangle = -i \int_{t_0}^{t} \mathrm{d}s\, g_1(s) \cdot \\ \cdot \langle [x^{(0)}(s),\, x^{(0)}(t)] \rangle Z_1(s-t), \quad (45)$$

where we have defined

$$Z_1(t-t') \equiv \langle \xi_1(t) \dot{\xi}_1(t') \rangle = \frac{\mathrm{d}}{\mathrm{d}t'} \mathcal{L}(t-t'), \quad (46)$$

where the decomposition in symmetric and antisymmetric contributions

$$Z_1(t-t') = Z_{1,\mathrm{s}}(t-t') + Z_{1,\mathrm{a}}(t-t'), \quad (47)$$

has been introduced, see Eq. (13). Finally, we arrive at the expression for the heat current

$$J_1 = -\int_{\bar{t}}^{\bar{t}+\mathcal{T}} \frac{\mathrm{d}s}{\mathcal{T}} \Big\{ \int_{t_0}^{s} \mathrm{d}s' g_1(s) g_1(s') F_1(s-s') \cdot \\ \cdot \langle x^{(0)}(s) x^{(0)}(s') \rangle - i \int_{t_0}^{s} \mathrm{d}s'\, g_1(s') g_1(s) \cdot \\ \cdot Z_1(s'-s) \langle [x^{(0)}(s'),\, x^{(0)}(s)] \rangle \Big\}. \quad (48)$$

To perform the average over $\mathcal{T}$ we observe that the correlation function

$$C(t,\, t') = \langle x^{(0)}(t) x^{(0)}(t') \rangle \quad (49)$$

only depends, in the long time limit $t \gg t_0$, on the time difference $t - t'$, i.e., in the long time limit $C(t,\, t') = C(t-t')$. This allows to change variable $\tau = s - s'$, to perform the limit $t_0 \to -\infty$, and thus to obtain

$$J_1 = -\frac{1}{2} \int_{0}^{+\infty} \mathrm{d}\tau \{ F_1(\tau) \cos(\Omega\tau) C(\tau) \\ - i Z_1(-\tau) \cos(\Omega\tau) [C(-\tau) - C(\tau)] \}. \quad (50)$$

By direct inspection one finds that $F_1(t) = -2i Z_{1,\mathrm{s}}(t)$ and introducing the response function $\chi_0(t) \equiv im\theta(t) \langle [x^{(0)}(t),\, x^{(0)}(0)] \rangle$ (see [108]) with $\theta(t)$ the Heaviside step function, whose Fourier transform is given in Eq. (28), it is then possible to rewrite the average heat current as in Eq. (26).

Turning to the average total power of Eq. (17), as detailed in Ref. [81], we have the general, exact expression

$$P = \int_{\bar{t}}^{\bar{t}+\mathcal{T}} \mathrm{d}s \Big\{ -\dot{g}_1(s) \langle x(s) \xi_1(s) \rangle \\ + \dot{g}_1(s) \Big\langle x(s) \int_{t_0}^{s} \mathrm{d}s'\, \gamma_1(s-s') \frac{\mathrm{d}}{\mathrm{d}s'} [g_1(s') x(s')] \Big\rangle \Big\}.$$

Following the same steps of the perturbative expansion detailed above, after the quantum average we get

$$P = \int_{\bar{t}}^{\bar{t}+\mathcal{T}} \frac{\mathrm{d}s}{\mathcal{T}} \Big\{ 2 \int_{t_0}^{s} \mathrm{d}s' \Big[\mathcal{L}_1(s'-s) \dot{g}_1(s) g_1(s') \cdot \\ \cdot C''(s-s') \Big] - \int_{t_0}^{s} \mathrm{d}s' \Big[\dot{g}_1(s) g_1(s') C(s-s') \cdot \\ \cdot \frac{\mathrm{d}}{\mathrm{d}s'} \gamma_1(s-s') \Big] + \gamma_1(0) \dot{g}_1(s) g_1(s) C(0) \Big\}. \quad (51)$$

Taking the average over the period of the drive, recalling Eqs. (13), (14), (15) and exploiting the identity $\dot{\gamma}_1(t) = -2i\mathcal{L}_{1,\mathrm{a}}(t)$ one obtains Eq. (25). Notice that the above results are fully consistent with those obtained using a fully non-equilibrium Green function formalism in the perturbative regime (see Appendix E of Ref. [78]).

Appendix A.2: Correlation functions

The auto–correlation function given in Sect. 2.2 can be evaluated in the perturbative regime following steps similar to those described above. Here we briefly outline the procedure to obtain D_{J_1}: Starting from the definition of Eq. (22), to lowest order it is sufficient to consider only the zero-th order term $x^{(0)}(t)$ of the position

operator $x(t)$ in Eq. (40). Then, the fluctuations of J_1 can be written as

$$D_{J_1}(t) = \int_0^{+\infty} \mathrm{d}\tau g_1(t) g_1(t-\tau) \cdot \cdot \left\langle \{x^{(0)}(t)\dot{\xi}_1(t),\, x^{(0)}(t-\tau)\dot{\xi}_1(t-\tau)\} \right\rangle.$$

The quantum averages in the above expression decouple in terms of the form $\langle x^{(0)}(t)x^{(0)}(t')\rangle \equiv C(t,\, t')$ – see Eq. (49) – and in terms of the form

$$\langle \dot{\xi}_1(t)\dot{\xi}_1(t')\rangle = \frac{\mathrm{d}}{\mathrm{d}t}\frac{\mathrm{d}}{\mathrm{d}t'}\mathcal{L}_1(t-t'). \tag{52}$$

Exploiting again the time translational invariance $C(t,\, t') = C(t-t')$ and following steps analogous to those discussed above, the fluctuations of J_1 averaged over $\mathcal{T}$ – see Eq. (23) – turn out to be Eq. (31). In complete analogy, we derive the period–averaged fluctuations of the power P in Eq. (30).

Appendix B: Operating modes

The operating modes of a thermal machine where the WM is connected to two thermal baths ($\nu = 1,\, 2$) can be classified studying the sign of the heat currents J_ν and of the total power P. Assuming $T_1 < T_2$, the only achievable modes in a two–terminal device are the two pure "heat engine" ($P < 0,\, J_1 < 0,\, J_2 > 0$) and "heat pump" modes ($P > 0,\, J_1 < 0,\, J_2 < 0$), the hybrid "refrigerator–pump" mode ($P > 0,\, J_1 > 0,\, J_2 < 0$), and the "wasteful" mode ($P > 0,\, J_1 < 0,\, J_2 > 0$) [33]. The latter is commonly labeled as "wasteful" [109, 110] since in this configuration heat flows from the hot bath at T_2 to the cold one at T_1 while the WM absorbs power. We note that other works [78, 111, 112] use different names for such operating modes, e.g., "dissipator" for "heat pump" and "accelerator" for "wasteful". We also use, in the main text, "refrigerator" in place of "refrigerator–pump" for shortness, although it actually corresponds to the hybrid mode where the machine simultaneously operates as refrigerator and heat pump. Indeed, the pure "refrigerator" mode can not be observed in a two–terminal device [110]. All the possible operating modes of the quantum thermal machine discussed in Sect. 3 are shown in Fig. 5 (see also Supplemental Information in Ref. [33]). We recall that, in this setup, the bath $\nu = 1$ is the Lorentzian bath with dynamical coupling, the bath $\nu = 2$ is the Ohmic bath with static coupling, and $J_2 = -P - J_1$ from Eq. (19).

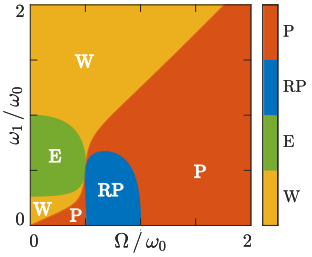

Fig. 5 Operating modes. All the possible operating modes of the quantum thermal machine discussed in main text as a function of the driving frequency Ω and the resonance frequency ω_1: Heat pump (P), refrigerator–pump (RP), heat engine (E), and wasteful (W). Parameters as in Fig. 2

References

1. M. Campisi, P. Hänggi, P. Talkner, Colloquium: quantum fluctuation relations: foundations and applications. Rev. Mod. Phys. **83**, 771 (2011)
2. R. Kosloff, Quantum thermodynamics: a dynamical viewpoint. Entropy **15**, 2100 (2013)
3. D. Gelbwaser-Klimovsky, W. Niedenzu, G. Kurizki, Thermodynamics of quantum systems under dynamical control. Adv. At. Mol. Opt. Phys. **64**, 329 (2015)
4. S. Vinjanampathy, J. Anders, Quantum thermodynamics. Contemp. Phys. **57**, 545 (2016)
5. P. Talkner, P. Hänggi, Colloquium: statistical mechanics and thermodynamics at strong coupling: quantum and classical. Rev. Mod. Phys. **92**, 041002 (2020)
6. G. Benenti, G. Casati, K. Saito, R.S. Whitney, Fundamental aspects of steady-state conversion of heat to work at the nanoscale. Phys. Rep. **694**, 1 (2017)
7. N.M. Myers, O. Abah, S. Deffner, Quantum thermodynamic devices: from theoretical proposals to experimental reality. AVS Quantum Sci. **4**, 027101 (2022)
8. B. Sothmann, R. Sánchez, A.N. Jordan, Thermoelectric energy harvesting with quantum dots. Nanotechnology **26**, 032001 (2015)
9. F. Giazotto, T.T. Heikkilä, A. Luukanen, A.M. Savin, J.P. Pekola, Opportunities for mesoscopics in thermometry and refrigeration: physics and applications. Rev. Mod. Phys. **78**, 217 (2006)
10. M.J. Martínez-Pérez, F. Giazotto, A quantum diffractor for thermal flux. Nat. Commun. **5**, 3579 (2014)
11. J.P. Pekola, B. Karimi, Colloquium: quantum heat transport in condensed matter systems. Rev. Mod. Phys. **93**, 041001 (2021)
12. L. Arrachea, Energy dynamics, heat production and heat-work conversion with qubits: toward the development of quantum machines. Rep. Prog. Phys. **86**, 036501 (2023)

13. P. Krantz, M. Kjaergaard, F. Yan, T.P. Orlando, S. Gustavsson, W.D. Oliver, A quantum engineer's guide to superconducting qubits. Appl. Phys. Rev. **6**, 021318 (2019)
14. A. Calzona, M. Carrega, Multi-mode architectures for noise-resilient superconducting qubits. Supercond. Sci. Technol. **36**, 023001 (2023)
15. A. Auffèves, Quantum technologies need a quantum energy initiative. PRX Quantum **3**, 020101 (2022)
16. G. Benenti, G. Casati, D. Rossini, G. Strini, *Principles of Quantum Computation and Information (A Comprehensive Textbook)* (World Scientific, Singapore, 2019)
17. I. Golokolenov et al., Thermodynamics of a single mesoscopic phononic mode. Phys. Rev. Res. **5**, 013046 (2023)
18. D. von Lindenfels et al., Spin heat engine coupled to a Harmonic-Oscillator flywheel. Phys. Rev. Lett. **123**, 080602 (2019)
19. L. M. Cangemi, C. Bhadra, A. Levy, Quantum engines and refrigerators. Arxiv:2302.00726 (2023)
20. J. Sheng, C. Yang, H. Wu, Realization of a coupled-mode heat engine with cavity-mediated nanoresonators. Sci. Adv. **7**, eabl7740 (2021)
21. F. Vischi, M. Carrega, P. Virtanen, E. Strambini, A. Braggio, F. Giazotto, Thermodynamic cycles in Josephson junctions. Sci. Rep. **9**, 3238 (2019)
22. J.Q. Quach et al., Superabsorption in an organic microcavity: toward a quantum battery. Sci. Adv. **8**, eabk3160 (2022)
23. I. Maillette de Buy-Wenniger et al., Coherence-powered work exchanges between a solid-state qubit and light fields. Arxiv:2202.01109 (2023)
24. B. Gardas, S. Deffner, A. Saxena, Non-hermitian quantum thermodynamics. Sci. Rep. **6**, 23408 (2016)
25. J.F.G. Santos, F.S. Luiz, Quantum thermodynamics aspects with a thermal reservoir based on $\mathcal{PT}$-symmetric Hamiltonians. J. Phys. A **54**, 335301 (2021)
26. A. Levy, R. Alicki, R. Kosloff, Quantum refrigerators and the third law of thermodynamics. Phys. Rev. E **85**, 061126 (2012)
27. F. Clivaz, R. Silva, G. Haack, J.B. Brask, N. Brunner, M. Huber, Unifying paradigms of quantum refrigeration: a universal and attainable bound on cooling. Phys. Rev. Lett. **123**, 170605 (2019)
28. J.-H. Jiang, O. Entin-Wohlman, Y. Imry, Thermoelectric three-terminal hopping transport through one-dimensional nanosystems. Phys. Rev. B **85**, 075412 (2012)
29. F. Mazza, R. Bosisio, G. Benenti, V. Giovannetti, R. Fazio, F. Taddei, Thermoelectric efficiency of three-terminal quantum thermal machines. New J. Phys. **16**, 085001 (2014)
30. F. Mazza, S. Valentini, R. Bosisio, G. Benenti, V. Giovannetti, R. Fazio, F. Taddei, Separation of heat and charge currents for boosted thermoelectric conversion. Phys. Rev. B. **91**, 245435 (2015)
31. P.A. Erdman, F. Mazza, R. Bosisio, G. Benenti, R. Fazio, F. Taddei, Thermoelectric properties of an interacting quantum dot based heat engine. Phys. Rev. B **95**, 245432 (2017)
32. J. Yang, C. Elouard, J. Splettstoesser, B. Sothmann, R. Sánchez, A.N. Jordan, Thermal transistor and thermometer based on Coulomb-coupled conductors. Phys. Rev. B **100**, 045418 (2019)
33. F. Cavaliere, L. Razzoli, M. Carrega, G. Benenti, M. Sassetti, Hybrid quantum thermal machines with dynamical couplings. iScience **26**, 106235 (2023)
34. R. López, J.S. Lim, K.W. Kim, Optimal superconducting hybrid machine. Phys. Rev. Res. **5**, 013038 (2023)
35. J. Lu, Z. Wang, R. Wang, J. Peng, C. Wang, J.-H. Jiang, Multitask quantum thermal machines and cooperative effects. Phys. Rev. B **107**, 075428 (2023)
36. B. Karimi, J.P. Pekola, Otto refrigerator based on a superconducting qubit: classical and quantum performance. Phys. Rev. B **94**, 184503 (2016)
37. J.P. Pekola, B. Karimi, G. Thomas, D.V. Averin, Supremacy of incoherent sudden cycles. Phys. Rev. B **100**, 085405 (2019)
38. K. Brandner, M. Bauer, U. Seifert, Universal coherence-induced power losses of quantum heat engines in linear response. Phys. Rev. Lett. **119**, 170602 (2017)
39. R. Kosloff, T. Feldmann, Discrete four-stroke quantum heat engine exploring the origin of friction. Phys. Rev. E **65**, 055102(R) (2002)
40. Y. Rezek, R. Kosloff, Irreversible performance of a quantum harmonic heat engine. New J. Phys. **8**, 83 (2006)
41. A. Friedenberger, E. Lutz, When is a quantum heat engine quantum? Europhys. Lett. **120**, 10002 (2017)
42. K. Korzekwa, M. Lostaglio, J. Oppenheim, D. Jennings, The extraction of work from quantum coherence. New J. Phys. **18**, 023045 (2016)
43. K. Hammam, H. Leitch, Y. Hassouni, G. De Chiara, Exploiting coherence for quantum thermodynamic advantage. New J. Phys. **24**, 113053 (2022)
44. P.A. Camati, J.F.G. Santos, R.M. Serra, Coherence effects in the performance of the quantum Otto heat engine. Phys. Rev. A **99**, 062103 (2019)
45. J. Liu, D. Segal, Coherences and the thermodynamic uncertainty relation: Insights from quantum absorption refrigerators. Phys. Rev. E **103**, 032138 (2021)
46. P. Chattopadhyay, A. Mitra, G. Paul, V. Zarikas, Bound on efficiency of heat engine from uncertainty relation viewpoint. Entropy **23**, 439 (2021)
47. G.T. Landi, M. Paternostro, Irreversible entropy production: from classical to quantum. Rev. Mod. Phys. **93**, 035008 (2021)
48. S. Hernández-Gómez et al., Experimental test of exchange fluctuation relations in an open quantum system. Phys. Rev. Res. **2**, 023327 (2020)
49. S. Hernández-Gómez, N. Staudenmaier, M. Campisi, N. Fabbri, Experimental test of fluctuation relations for driven open quantum systems with an NV center. New J. Phys. **23**, 065004 (2021)
50. A.C. Barato, U. Seifert, Thermodynamic uncertainty relation for biomolecular processes. Phys. Rev. Lett. **114**, 158101 (2015)
51. N. Shiraishi, K. Saito, H. Tasaki, Universal trade-off relation between power and efficiency for heat engines. Phys. Rev. Lett. **117**, 190601 (2016)
52. A.M. Timpanaro, G. Guarnieri, J. Goold, G.T. Landi, Thermodynamic uncertainty relations from exchange

fluctuation theorems. Phys. Rev. Lett. **123**, 090604 (2019)
53. G. Guarnieri, G.T. Landi, S.R. Clark, J. Goold, Thermodynamics of precision in quantum nonequilibrium steady states. Phys. Rev. Res. **1**, 033021 (2019)
54. Y. Hasegawa, Thermodynamic uncertainty relation for general open quantum systems. Phys. Rev. Lett. **126**, 010602 (2021)
55. S. Pal et al., Experimental study of the thermodynamic uncertainty relation. Phys. Rev. Res. **2**, 022044 (2020)
56. N. Shiraishi, K. Saito, Fundamental relation between entropy production and heat current. J. Stat. Phys. **174**, 433 (2019)
57. L.M. Cangemi, M. Carrega, A. De Candia, V. Cataudella, G. De Filippis, M. Sassetti, G. Benenti, Optimal energy conversion through antiadiabatic driving breaking time-reversal symmetry. Phys. Rev. Res. **3**, 013237 (2021)
58. P. Menczel, E. Loisa, K. Brandner, C. Flindt, Thermodynamic uncertainty relations for coherently driven open quantum systems. J. Phys. A **54**, 314002 (2021)
59. T. Koyuk, U. Seifert, Thermodynamic uncertainty relation for time-dependent driving. Phys. Rev. Lett. **125**, 260604 (2020)
60. E. Potanina, C. Flindt, M. Moskalets, K. Brandner, Thermodynamic bounds on coherent transport in periodically driven conductors. Phys. Rev. X **11**, 021013 (2021)
61. G. T. Landi, M. J. Kewming, M. T. Mitchison, P. P. Potts, Current fluctuations in open quantum systems: Bridging the gap between quantum continuous measurements and full counting statistics. arXiv:2303.04270 (2023)
62. J.M. Horowitz, T.R. Gingrich, Proof of the finite-time thermodynamic uncertainty relation for steady-state currents. Phys. Rev. E **96**, 020103 (2017)
63. P. Pietzonka, U. Seifert, Universal trade-off between power, efficiency, and constancy in steady-state heat engines. Phys. Rev. Lett. **120**, 190602 (2018)
64. T. Koyuk, U. Seifert, P. Pietzonka, A generalization of the thermodynamic uncertainty relation to periodically driven systems. J. Phys. A **52**, 02LT02 (2019)
65. K. Brandner, T. Hanazato, K. Saito, Thermodynamic bounds on precision in ballistic multiterminal transport. Phys. Rev. Lett. **120**, 090601 (2018)
66. K. Ptaszyński, Coherence-enhanced constancy of a quantum thermoelectric generator. Phys. Rev. B **98**, 085425 (2018)
67. L.M. Cangemi, V. Cataudella, G. Benenti, M. Sassetti, G. De Filippis, Violation of thermodynamics uncertainty relations in a periodically driven work-to-work converter from weak to strong dissipation. Phys. Rev. B **102**, 165418 (2020)
68. G. Benenti, G. Casati, J. Wang, Power, efficiency, and fluctuations in steady-state heat engines. Phys. Rev. E **102**, 040103(R) (2020)
69. V. Singh, V. Shaghaghi, Ö. E. Müstecaplıoğlu, D. Rosa, Thermodynamic uncertainty relation in nondegenerate and degenerate maser heat engines. ArXiv:2211.08377 (2023)
70. H.J.D. Miller, M.H. Mohammady, M. Perarnau-Llobet, G. Guarnieri, Thermodynamic uncertainty relation in slowly driven quantum heat engines. Phys. Rev. Lett. **126**, 210603 (2021)
71. M. Aspelmeyer, T.J. Kippenberg, F. Marquardt, Cavity optomechanics. Rev. Mod. Phys. **86**, 1391 (2014)
72. S. Barzanjeh, A. Xuereb, S. Gröblacher, M. Paternostro, C.A. Regal, E.M. Weig, Optomechanics for quantum technologies. Nat. Phys. **18**, 15 (2022)
73. A. Cottet et al., Cavity QED with hybrid nanocircuits: from atomic-like physics to condensed matter phenomena. J. Phys. **29**, 433002 (2017)
74. C. Zherbe, P. Hänggi, Phys. Rev. E **52**, 1533 (1995)
75. A. Blais, R.-S. Huang, A. Wallraff, S.M. Girvin, R.J. Schoelkopf, Phys. Rev. A **69**, 062320 (2004)
76. S. Barzanjeh, M. Aquilina, A. Xuereb, Manipulating the flow of thermal noise in quantum devices. Phys. Rev. Lett. **120**, 060601 (2018)
77. A. Pontin, H. Fu, J.H. Iacoponi, P.F. Barker, T.S. Monteiro, Controlling mode orientations and frequencies in levitated cavity optomechanics. Phys. Rev. Res. **5**, 013013 (2023)
78. F. Cavaliere, M. Carrega, G. De Filippis, V. Cataudella, G. Benenti, M. Sassetti, Dynamical heat engines with non-Markovian reservoirs. Phys. Rev. Res. **4**, 033233 (2022)
79. U. Weiss, *Quantum Dissipative Systems*, 5th edn. (World Scientific, Singapore, 2021)
80. A.O. Caldeira, A.J. Leggett, Quantum tunnelling in a dissipative system. Ann. Phys. **149**, 374 (1983)
81. M. Carrega, L.M. Cangemi, G. De Filippis, V. Cataudella, G. Benenti, M. Sassetti, Engineering dynamical couplings for quantum thermodynamic tasks. PRX Quantum **3**, 010323 (2022)
82. M. Thorwart, E. Paladino, M. Grifoni, Dynamics of the spin-boson model with a structured environment. Chem. Phys. **296**, 333 (2004)
83. E. Paladino, A.G. Maugeri, M. Sassetti, G. Falci, U. Weiss, Structured environments in solid state systems: crossover from Gaussian to non-Gaussian behavior. Phys. E **40**, 198 (2007)
84. J. Iles-Smith, N. Lambert, A. Nazir, Environmental dynamics, correlations, and the emergence of noncanonical equilibrium states in open quantum systems. Phys. Rev. A **90**, 032114 (2014)
85. P. Strasberg, G. Schaller, N. Lambert, T. Brandes, Nonequilibrium thermodynamics in the strong coupling and non-Markovian regime based on a reaction coordinate mapping. New J. Phys. **18**, 073007 (2016)
86. S. Restrepo, J. Cerrillo, P. Strasberg, G. Schaller, From quantum heat engines to laser cooling: Floquet theory beyond the Born-Markov approximation. New J. Phys. **20**, 053063 (2018)
87. M. Wiedmann, J.T. Stockburger, J. Ankerhold, Non-Markovian dynamics of a quantum heat engine: out-of-equilibrium operation and thermal coupling control. New J. Phys. **22**, 033007 (2020)
88. K. Ptaszyński, M. Esposito, Entropy production in open systems: the predominant role of intraenvironment correlations. Phys. Rev. Lett. **123**, 200603 (2019)
89. J. Liu, K.A. Jung, D. Segal, Periodically driven quantum thermal machines from warming up to limit cycle. Phys. Rev. Lett. **127**, 200602 (2021)
90. K. Brandner, U. Seifert, Periodic thermodynamics of open quantum systems. Phys. Rev. E **93**, 062134 (2016)

91. N. Freitas, J.P. Paz, Fundamental limits for cooling of linear quantum refrigerators. Phys. Rev. E **95**, 012146 (2017)
92. N. Freitas, J.P. Paz, Cooling a quantum oscillator: a useful analogy to understand laser cooling as a thermodynamical process. Phys. Rev. A **97**, 032104 (2018)
93. L. Arrachea, E.R. Mucciolo, C. Chamon, R.B. Capaz, Microscopic model of a phononic refrigerator. Phys. Rev. B **86**, 125424 (2012)
94. B. Peropadre, D. Zueco, F. Wulschner, F. Deppe, A. Marx, R. Gross, J.J. García-Ripoll, Tunable coupling engineering between superconducting resonators: from sidebands to effective gauge fields. Phys. Rev. B **87**, 134504 (2013)
95. F. Wulschner et al., Tunable coupling of transmission-line microwave resonators mediated by an rf SQUID. EPJ Quant. Technol. **3**, 10 (2016)
96. B.K. Agarwalla, D. Segal, Assessing the validity of the thermodynamic uncertainty relation in quantum systems. Phys. Rev. B **98**, 155438 (2018)
97. J. Roßnagel, O. Abah, F. Schmidt-Kaler, K. Singer, E. Lutz, Nanoscale heat engine beyond the Carnot limit. Phys. Rev. Lett. **112**, 030602 (2014)
98. J. Klaers, S. Faelt, A. Imamoglu, E. Togan, Squeezed thermal reservoirs as a resource for a nanomechanical engine beyond the Carnot limit. Phys. Rev. X **7**, 031044 (2017)
99. B.K. Agarwalla, J.-H. Jiang, D. Segal, Quantum efficiency bound for continuous heat engines coupled to noncanonical reservoirs. Phys. Rev. B **96**, 104304 (2017)
100. G. Manzano, F. Galve, R. Zambrini, J.M.R. Parrondo, Entropy production and thermodynamic power of the squeezed thermal reservoir. Phys. Rev. E **93**, 052120 (2016)
101. G. Manzano, Squeezed thermal reservoir as a generalized equilibrium reservoir. Phys. Rev. E **98**, 042123 (2018)
102. R. Long, W. Liu, Performance of quantum Otto refrigerators with squeezing. Phys. Rev. E **91**, 062137 (2015)
103. V. Singh, Ö.E. Müstecaplıoğlu, Performance bounds of nonadiabatic quantum harmonic Otto engine and refrigerator under a squeezed thermal reservoir. Phys. Rev. E **102**, 062123 (2020)
104. O. Abah, E. Lutz, Efficiency of heat engines coupled to nonequilibrium reservoirs. EPL **106**, 20001 (2014)
105. R. Alicki, D. Gelbwaser-Klimovsky, Non-equilibrium quantum heat machines. New J. Phys. **17**, 115012 (2015)
106. W. Niedenzu, D. Gelbwaser-Klimovsky, A.G. Kofman, G. Kurizki, On the operation of machines powered by quantum non-thermal baths. New J. Phys. **18**, 083012 (2016)
107. W. Niedenzu, V. Mukherjee, A. Ghosh, A.G. Kofman, G. Kurizki, Quantum engine efficiency bound beyond the second law of thermodynamics. Nat. Commun. **9**, 165 (2018)
108. G.F. Giuliani, G. Vignale, *Quantum Theory of the Electron Liquid* (Cambridge University Press, Cambridge, 2005)
109. F. Hajiloo, R. Sánchez, R.S. Withney, J. Splettstoesser, Quantifying nonequilibrium thermodynamic operations in a multiterminal mesoscopic system. Phys. Rev. B **102**, 155405 (2020)
110. G. Manzano, R. Sánchez, R. Silva, G. Haack, J.B. Brask, N. Brunner, P.P. Potts, Hybrid thermal machines: generalized thermodynamic resources for multitasking. Phys. Rev. Res. **2**, 043302 (2020)
111. L. Buffoni, A. Solfanelli, P. Verrucchi, A. Cuccoli, M. Campisi, Quantum measurement cooling. Phys. Rev. Lett. **122**, 070603 (2019)
112. A. Solfanelli, M. Falsetti, M. Campisi, Nonadiabatic single-qubit quantum Otto engine. Phys. Rev. B **101**, 054513 (2020)